Applied Surface Science 352 (2015) 109–116

Contents lists available at ScienceDirect

Applied Surface Science

journal homepage: www.elsevier.com/locate/apsusc

Structural characterization of copolymer embedded magnetic nanoparticles

G.G. Nedelcu[a,*], A. Nastro[b], L. Filippelli[b], M. Cazacu[c], M. Iacob[c], C. Oliviero Rossi[b], A. Popa[d], D. Toloman[d], M. Dobromir[a], F. Iacomi[a]

[a] Faculty of Physics, University "Alexandru Ioan Cuza", Carol I Bulevard, Nr.11, 700506 Iasi, Romania
[b] Department of Chemistry and Chemical Technology, University of Calabria, Via P. Bucci, 87036 Arcavacata di Rende, Cosenza, Italy
[c] Institute of Macromolecular Chemistry "Petru Poni", Aleea Grigore Ghica Voda, nr. 41A, 700487 Iasi, Romania
[d] National Institute for Research and Development of Isotopic and Molecular Technologies, 65-103 Donath Str., 400293 Cluj-Napoca 5, Romania

ARTICLE INFO

Article history:
Received 26 January 2015
Received in revised form 23 April 2015
Accepted 25 April 2015
Available online 14 May 2015

Keywords:
Magnetic nanoparticles
Polymer coating
Ageing effect

ABSTRACT

Small magnetic nanoparticles (Fe_3O_4) were synthesized by co-precipitation and coated by emulsion polymerization with poly(methyl methacrylate-co-acrylic acid) (PMMA-co-AAc) to create surface functional groups that can attach drug molecules and other biomolecules. The coated and uncoated magnetite nanoparticles were stored for two years in normal closed ships and than characterized by Fourier transform infrared spectroscopy, X-ray diffraction, transmission electron microscopy, vibrating sample magnetometry, and electron paramagnetic resonance spectroscopy. The solid phase transformation of magnetite to maghemite, as well as an increase in particle size were evidenced for the uncoated nanoparticles. The coated nanoparticles preserved their magnetite structure and magnetic properties. The influences of monomers and surfactant layers on interactions between the magnetic nanoparticles evidenced that the thickness of the polymer has a significant effect on magnetic properties.

1. Introduction

Magnetic nanoparticles (MPs) have been used frequently lately in medical applications such as contrast agents in magnetic resonance imaging [1–8], magnetic fluid hyperthermia for treatment of tumors [9–15], agents for targeted drug release [16–19], detoxification of biological fluids [20], tissue repair [21], magnetic separation of blood components [22–24], biosensors [25], immunoassay [26], and so on. These particles have a high magnetic susceptibility and high coercitivity, they also are nontoxic to the body's internal environment and production costs are low. Another aspect that should not be neglected is that their surface can be modified easily by creating a layer of polymer that can be functionalized with various drugs and biomolecules.

The methods generally used for synthesizing MPs are: emulsion polymerization [27], chemical coprecipitation [28–30], forced hydrolysis [31], sol–gel with auto-combustion [32,33], and microwave plasma [34]. Form all these methods, chemical coprecipitation seems to be the most productive, simple, and cheap. This method enables to control several parameters (temperature and pH) in order to obtain desired particle sizes and shapes [35].

The combination magnetic particle-poly(methyl methacrylate) (PMMA) is used in several biomedical applications such as magnetic fluid hyperthermia, magnetic separations, and thermosensitive drug delivery. So far, in the literature, were made a number of attempts for embedding MPs in PMMA. Some authors investigated PMMA stabilized colloidal metallic iron particles without additional surfactant or stabilizer and have found that particle sizes and properties were strongly dependent on polymer concentration [36]. Others revealed that the change in the stirring rate and solution pH plays an important role in controlling the particle size and that the concentration of the base (sodium hydroxide) and temperature values have no significant effect [37–39]. It was proved that the rate of drug release from the particles coated with pH-sensitive poly((2-dimethylamino) ethyl methacrylate) (PDMAEMA) could be effectively controlled by altering the pH values of the environment and that magnetic nanoparticles coated with PMMA exhibit an improved dispersibility in organic solvents and have interesting magnetic properties [40,41].

The altering interfacial properties of magnetite nanoparticles in aqueous dispersions, which contribute to the change in their colloidal stability was also analyzed by some authors [42,43]. It was evidenced that in aged magnetite nanoparticles stored in aqueous

* Corresponding author. Tel.: +40 742872871.
E-mail address: ggnedelcu@yahoo.com (G.G. Nedelcu).

http://dx.doi.org/10.1016/j.apsusc.2015.04.191
0169-4332/

medium a solid phase transformation of magnetite to maghemite takes place.

In this report we are focused on the characterization of as-synthesized and 2 years aged magnetic nanoparticles, uncoated and coated with PMMA-co-AAc copolymer for possible medical applications.

2. Materials and methods

2.1. Preparation of magnetic nanoparticles (MP)

Magnetic nanoparticles were prepared by co-precipitation of the ferrous chloride ($FeCl_2 \cdot 4H_2O$) and the ferric chloride ($FeCl_3 \cdot 6H_2O$) solutions, choosing a molar ratio of Fe^{2+}:Fe^{3+} = 1:2 and using an alkaline sodium hydroxide (NaOH) solution [37]. Our reaction equipment consisted of a flat bottom flask and an overhead stirrer. In a reactor containing 160 ml distilled water at 80 °C were added through vigorous agitation (stirring rate was 1000 rot/min) aqueous solutions containing Fe^{2+} and Fe^{3+} salts (120 ml aqueous solution, total 1.25 M) and NaOH (and 120 ml of 5 M). The black precipitate was formed at the early phase, but the medium was continuously stirred for 2 h at pH = 12, maintaining the stirring rate, the temperature and adding slowly 10 ml 25% (w/w) tetramethylammonium hydroxide (TMAOH) to stabilize the MPs. No inert atmosphere or deaerated aqueous solutions were used in order to induce the formation of a single iron oxide magnetite phase.

2.2. Synthesis of magnetic polymeric particles (MPPs)

The magnetic particles produced with a recipe above mentioned were selected (sample MP, Table 1) and a part of them were used in a second step, in which they were coated with acrylic polymers containing carboxylic acid functional groups. The coating of the nanoparticles was carried out by emulsion polymerization, at two different surfactant to monomer ratios and a co-monomer weight ratio of 90/10, in an oil-in-water (o/w) system (samples MPP1, MPP2, Table 1).

In order to obtain the polymer coated nanoparticles, MPP1 and MPP2, to the magnetic suspension (2% wt) previously synthesized was added, as a surfactant, 10 ml of 4% or 2% respectively sodium dodecyl sulfate (SDS) solution and 50 ml of a 4% or 8% respectively co-monomer mixture, mixing the dispersion for about 15 min. After the addition of 5 ml 2% potassium persulfate (KPS), as an initiator, the polymerization was carried out in a constant temperature shaking bath at 65 °C for 24 h.

Table 1
Reaction parameters and sample codes.

Experiment	Surfactant concentration SDS (%)	Initiator concentration KPS (%)	Co-monomers concentration MMA + AAc (%)	pH	Temperature (°C)	Stirring rate (rpm)
MP	–	–	–	–	–	–
MPP1	4	2	4	8	65	300
MPP2	2	2	8	8	65	300

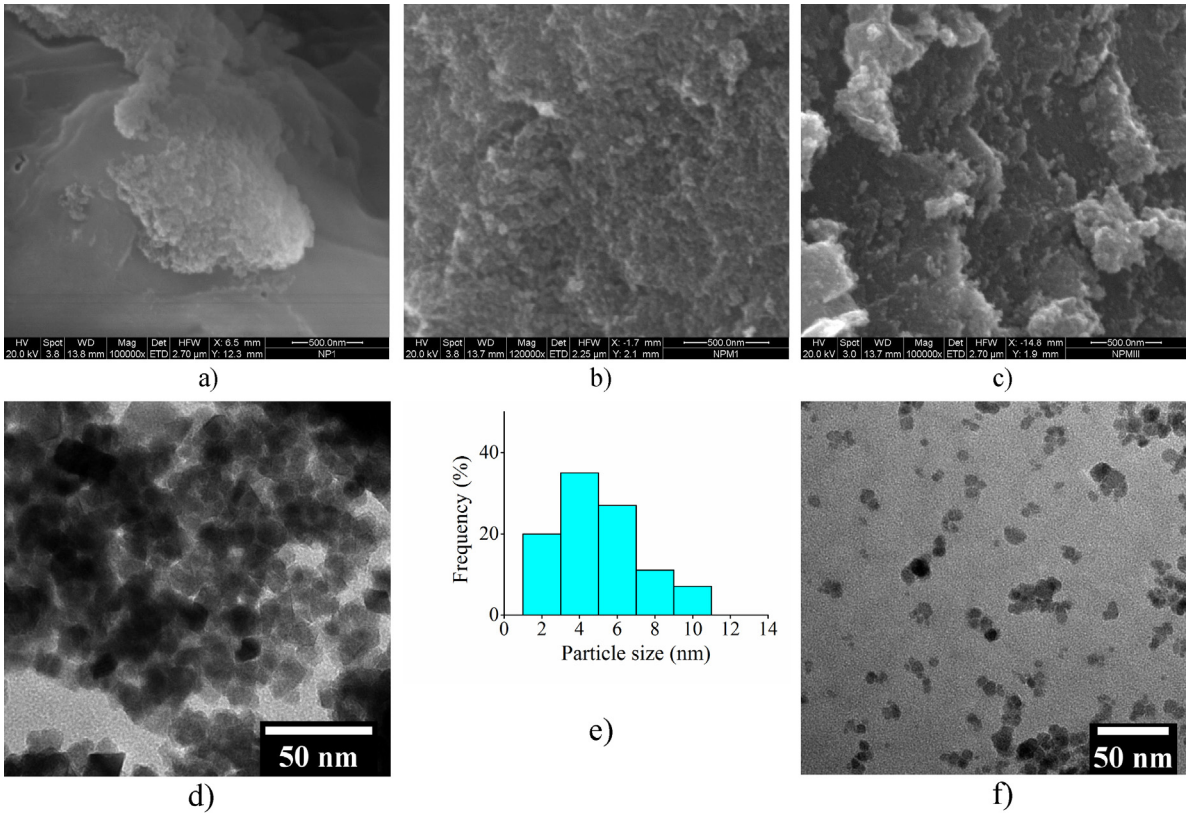

Fig. 1. SEM images of nanoparticles: (a) uncoated MP, (b) polymer coated MPP1, (c) polymer coated MPP2. TEM images of aged nanoparticles: (d) uncoated MPa, (e) particle size distribution of polymer coated MPP1a, (f) polymer coated MPP2a.

Due to the fact that the acrylic acid (AAc) is very soluble in water in comparison with the solubility of methyl methacrylate (MMA), the SDS stabilized microdroplets may contain a lower percent of acrylic acid in comparison with the starting MMA–AAc mixtures, a consequence of the migration of acrylic acid from the oil phase to the aqueous phase, but enough to form carboxylic acid functional groups on the surface of the magnetic polymeric particles [44]. A consequence of the acrylic acid solubility in water may be the acidification of the aqueous medium which can start to dissolve the iron oxide nanoparticles resulting a soluble iron acrylate and a mass loss of nanoparticles. To prevent this process, the pH of the reaction medium was maintained at 8 by the addition of sodium hydroxide.

After the polymerization, the coated magnetic nanoparticles were cleaned by washing with methanol and water several times to remove the unreacted monomers and the surfactant. The magnetic particles were collected with the help of a magnet and washed with distilled water. The so obtained particles were placed in 0.1 M of H_2SO_4 solution for 24 h to separate the possible uncoated nanoparticles. The sulfuric acid treatment attacks only the magnetic cores of MPs without harming the coated magnetic nanoparticles whose polymeric layer is impermeable. Finally, the uncoated and polymer-coated particles were washed with deionized water, dried at 40 °C and aged in closed ships for 2 years in (MPa, MPP2a).

3. Results and discussions

3.1. Structural and morphological investigations of as synthesized and aged nanoparticles

The as synthesized (MP, MPP1, MPP2) and aged nanoparticles (MPa, MPP1a, MPP2a) were structurally analyzed using Fourier transform infrared (FTIR) spectroscopy (Bruker Vertex 70) scanning electron microscopy (SEM), transmission electron microscopy (TEM), and X-ray diffraction.

The SEM images of as synthesized nanoparticles, MP, MPP1, MPP2, are show in Fig. 1. SEM image of dried uncoated nanoparticles shows agglomerations of 20–40 nm of very small nanoparticles (3–7 nm) with a nearly spherical shape (Fig. 1a). SEM images of dried polymer coated nanoparticles, with ratio surfactant/comonomer values 1 and 0.25, show agglomerations of 30–50 nm of polymer coated small nanoparticles (4–8 nm, Fig. 1b and 7–11 nm Fig. 1c).

It is known that due to their hydrophylic character, the iron oxide nanoparticles have a higher affinity for water phase and a much lower for the oily (MMA-based) phase, and thus it seems that the polymer encapsulation must be very low and the coating must be inhomogeneous. In reality, due to the adsorption of dodecylsulfate ions on their surface (which are oriented with the negative sulfate group towards the $[N(CH_3)_4]^+$ ions, previously adsorbed to

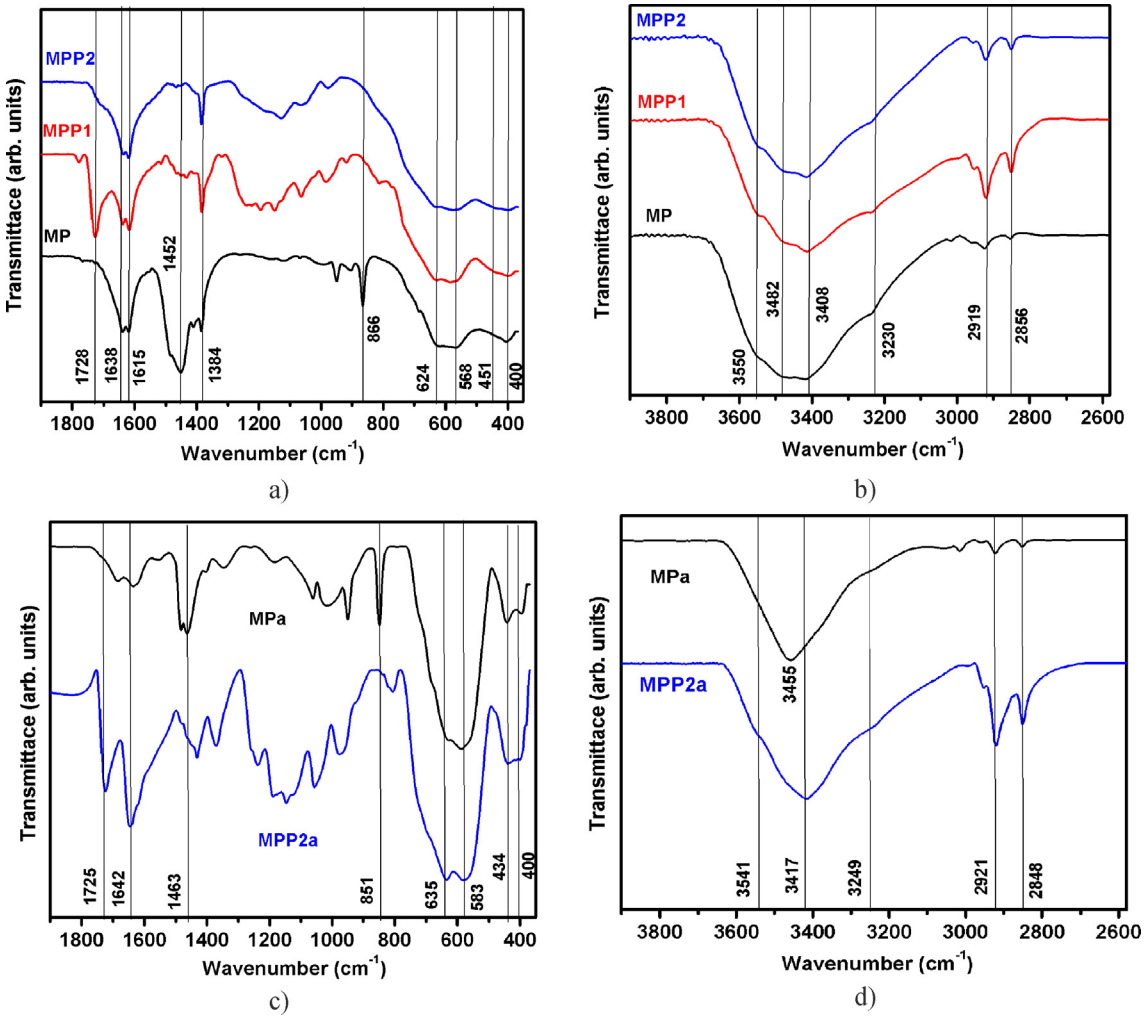

Fig. 2. FTIR spectra of: (a, b) as synthesized nanoparticles and (c, d) aged nanoparticles.

Table 2
The main values of vibrational bands shown in FTIR spectra for uncoated and coated magnetic nanoparticles.

Sample	OH, H_2O deformation		Vibration band (cm^{-1})						
			C–H CH_2	C=O in carbonyl	CH_3 bending	C–O–C in ester	C–C in polymeric chain	Tetrahedral metal–oxygen	Octahe-dral metal–oxygen
MP	3439	1619						572	390
								624	440
MPa	3459	1620						583	395
								627	440
MPP1	3439	1617	2921	1728	1384	1125	977	583	399
								630	436
MPP2	3432	1619	2921		1384	1122	975	575	398
								629	436
MPP2a	3415	1620	2919	1725	1370	1119	973	586	400
								633	437

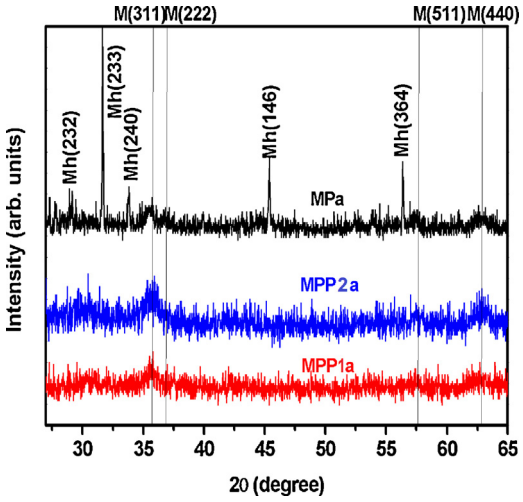

Fig. 3. XRD patterns of aged magnetic nanoparticles: uncoated (MPa) and coated with PMMA (MPP1a, MPP2a).

iron oxide surface and the dodecyl nonpolar long chain to external medium) the SDS-coated Fe oxide nanoparticles were easily trapped inside MMA-based oily droplets where the majority of the polymerization processes occurred [45].

The investigation of 2 years aged nanoparticles by TEM evidenced an increase in uncoated nanoparticle sizes (mean size value of 8 nm) (MPa, Fig. 1d) and that the aggregation of nanoparticles determined the formation in time of some big crystalline particles (mean size value of 90 nm). TEM images of polymer coated nanoparticles MPP1a (mean size value of 5 nm, Fig. 1e) and MPP2a (mean size value of 6 nm, Fig. 1f) show an unchanged morphology.

The infrared spectroscopy is a useful tool for the identification of iron oxide phases because the spectrum arises as a result of divalent and trivalent cations interaction with electromagnetic radiation. The FTIR bands at 570 and 390 cm^{-1} were assigned to the Fe–O vibration modes of tetrahedral and octahedral sites and in octahedral sites respectively, in Fe_3O_4. The positions of these two bands depend on the stoichiometry of magnetite. The split of these bands determines the apparition of two new bands at 430 and 630 cm^{-1} indicating an increase in cation vacancy in the lattice [46].

The FTIR spectra of as-synthesized magnetic nanoparticles, shown in Fig. 2a, evidence the vibration bands typical for non-stoichiometric magnetite at 400, 451, 568, and 624 cm^{-1}. The interaction between magnetite and polymer layer induces a shift of magnetite characteristic peaks to higher wavenumbers as a function of the surfactant/polymer ratio (Table 2). Moreover, the FTIR spectra of as synthesized nanoparticles (Fig. 2a, b) evidence the vibration bands belonging to CO_3 group, around 866, 1450 cm^{-1}, resulted from the decomposition of tetramethylammonium hydroxide and the vibration bands at 3230, 3403, 3482, 3550, and 1620 cm^{-1}, assigned to stretching vibrations and bending vibrations of adsorbed water on the surface of the iron oxide nanoparticles and OH stretching in carboxylic acid groups.

The FTIR spectra of copolymer coated nanoparticles MPP2 (Fig. 2a, b) contains also the vibration bands typical for the AAc-co-MMA, at 2856–2912 cm^{-1} (CH stretchig in CH_2, CH_3 grups), 1728 cm^{-1} (C=O stretching in carbonyl groups), 1384 cm^{-1} (CH_3 bending vibration), 1125 cm^{-1} (C–O–C vibration in ester groups), and 977 cm^{-1} (C–C stretching). Due to the higher ratio surfactant/copolymer in sample MPP1, the FTIR spectrum evidences the vibration bands typical for the SDS (1232 cm^{-1} vibration in SO_2) [37].

The FTIR spectra of aged nanoparticles (Fig. 2c, d) show a major loss in water content in comparison to the as prepared ones. Due to the water loss the vibration bands attributed to the copolymer are more visible. A diminution in the split of the vibration band attributed to Fe–O in tetrahedral and octahedral sites and the diminution in the intensity of vibration band at around 400 nm indicate the presence of maghemite phase.

The crystalline structure of the aged magnetic nanoparticles was investigated by X-ray diffraction (XRD) using an AD8 Bruker ADVANCE diffractometer. Fig. 3 and Table 3 show the XRD patterns and the structural parameters of uncoated (MPa) and polymer

Table 3
Nanoparticle structural parameters as determined from XRD patterns and XPS spectra (*a*, constant of the network; *D*, crystallite size; M, cubic magnetite; Mh, cubic maghemite).

Sample code		Phase (%)		*a* (nm)		*D* (nm)		Fe^{2+}/Fe^{3+}	Fe_o^{3+} (%)		Fe_t^{3+} (%)	
		M	Mh	M	Mh	D_{331}	D_{300}	M	M	Mh	M	Mh
MPa	XRD	31.0	69.0	0.835	0.835	11	108					
	XPS	30.4	69.6			8		0.500	67	65	33	35
MPP1a	XRD	100		0.834		7						
	XPS					5		0.50	70		30	
MPP2a	XRD	100		0.833		8						
	XPS					5		0.499	74		26	

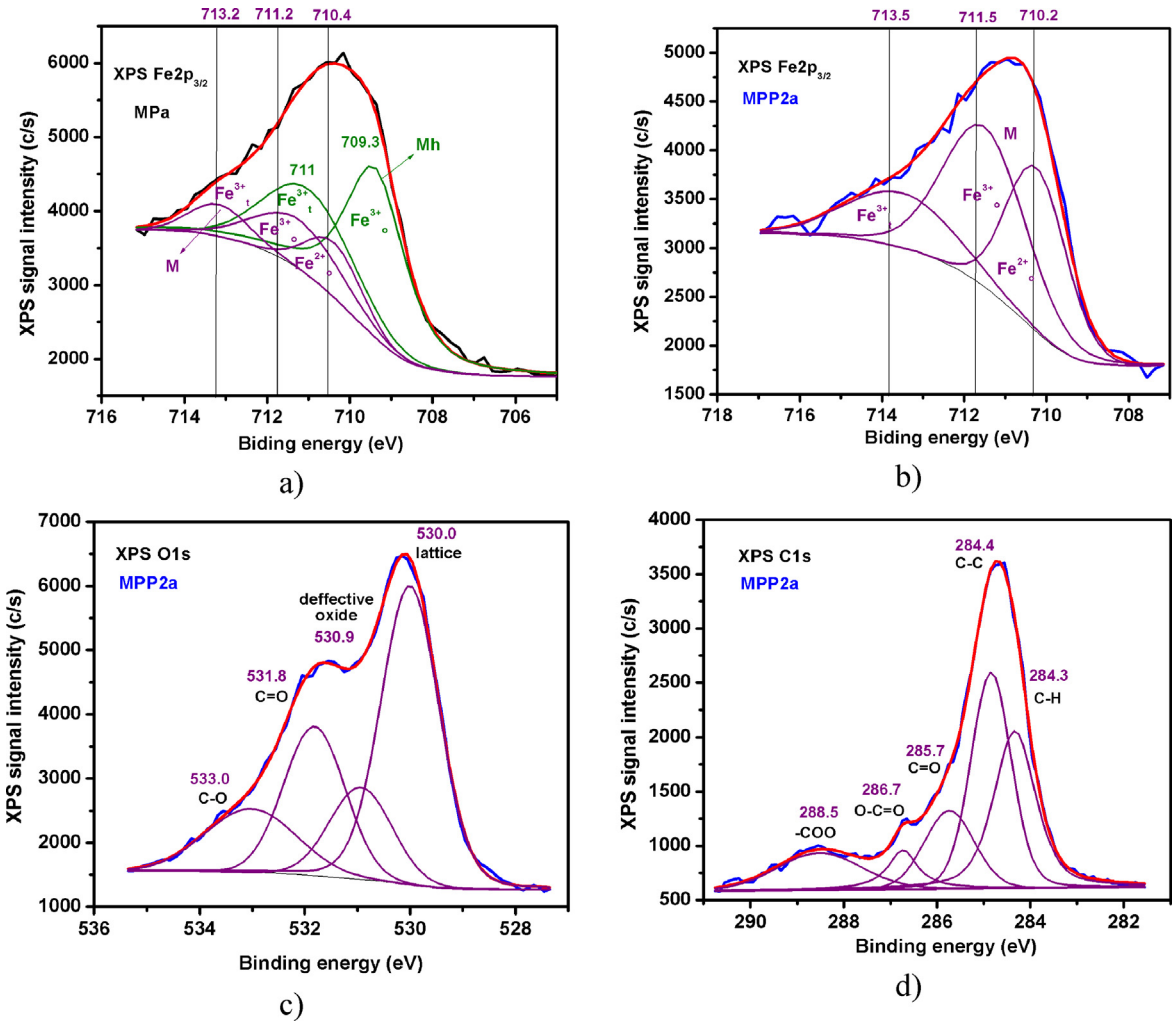

Fig. 4. XPS spectra of aged nanoparticles: (a) Fe $2p_{3/2}$ in Mpa, (b) Fe $2p_{3/2}$ in MPP2a, (c) O1s in MPP2a, and (d) C1s in MPP2a.

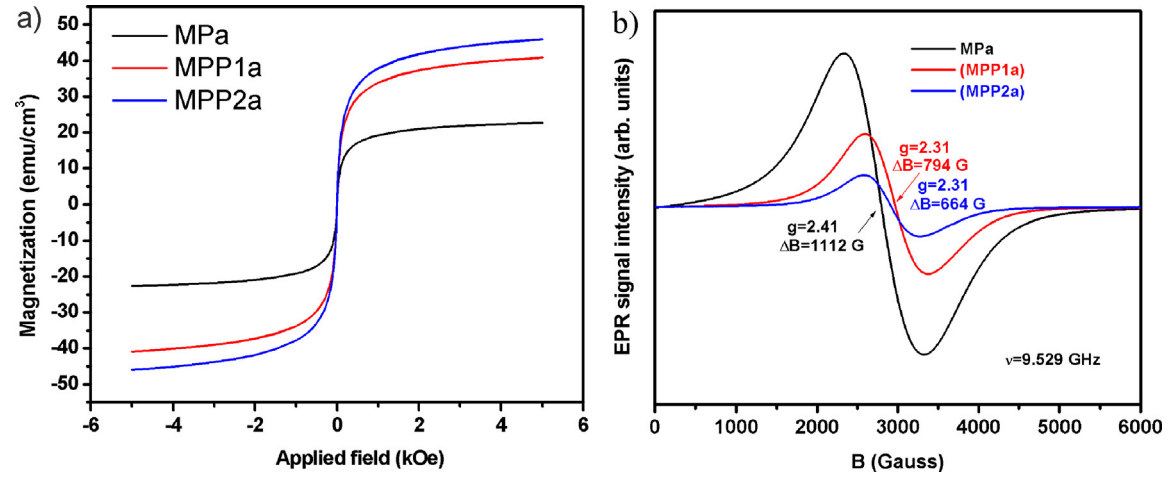

Fig. 5. Room temperature magnetic properties of aged nanoparticles: (a) hysteresis loops and (b) EPR spectra in X band.

coated nanoparticles (MPP1a, MPP2a). The XRD pattern of the aged uncoated nanoparticles shows two types of nanoparticles: ones having small sizes (11 nm) and the cubic spinel structure of magnetite (Fe_3O_4) and others having big sizes (100 nm) and the cubic structure of maghemite (γ-Fe_2O_3). The content in maghemite was found to be of 69%. In time, in the uncoated nanoparticles, Fe^{2+} can oxidate to Fe^{3+}, thus the final composition being a mixture of magnetite and maghemite phases.

The XRD patterns of aged copolymer coated nanoparticles, MPP1a and MPP2a, show only the diffraction peaks of spinel structure typical for magnetite and only small nanoparticles, in agreement with TEM investigations. The small values found for the

unit cell parameter indicate structural defects in good agreement with FTIR results.

Compositional analysis of the aged nanoparticles was determined using X-ray photoelectron spectroscopy (XPS, PHY-ULVAC VersaProbe 5000, AlKα source, 1486.6 eV). The binding energy scale was charge referenced to the C 1s at 284.6 eV [19].

The high-resolution narrow-scan XPS spectra of Fe 2p, O 1s, and C1s peaks of nanoparticles are shown in Fig. 4.

The Fe2p XPS spectra of MPP1a and MPP2a samples evidenced the magnetite characteristic peaks located at 711 and 724.6 eV, corresponding to Fe $2p_{3/2}$ and Fe $2p_{1/2}$ respectively. The Fe 2p spectrum of MPa sample was shifted to lower biding energy, with peaks located at 710.3 and 723.7 eV, suggesting important maghemite content. The peak shape for Fe $2p_{3/2}$ XPS spectra revealed the presence of two nonequivalent bonds of Fe ions attributed to octahedral (Fe_o^{3+}) and tetrahedral (Fe_t^{3+}) lattice sites for Fe^{3+}. In magnetite Fe^{2+} is located only in octahedral sites (Fe_o^{2+}). The decomposition of Fe $2p_{3/2}$ peak in its components allowed the determination of magnetite content by taking into consideration the following peaks: 710.2 eV for Fe_o^{2+}, 711.5 eV for Fe_o^{3+}, and 713.5 eV for Fe_t^{3+}. The $2p_{3/2}$ components for Fe_o^{3+} Fe_t^{3+} in maghemite were 709.3 and 710.98 eV respectively. The Fe^{2+}/Fe^{3+} ratio in magnetite and the relative contributions of Fe^{3+} ions in octahedral and tetrahedral sites were determined by fitting the spectral line with XPSPEAK41 program (Table 3). A diminution in the content of Fe_t^{3+} lattice sites was evidenced due to the interaction with the copolymer. The concentration in maghemite phase was found to be 69.6%, very close to the value obtained from XRD.

Table 4
Magnetic parameters of aged uncoated and copolymer coated nanoparticles.

Sample	M_s (emu/cm^3)	M_r (emu/cm^3)	H_c (Oe)	M_r/M_s	g	ΔB (G)
MPa	22.7	0.769	−0.002	0.034	2.41	1012
MPP1a	41.0	1.214	−0.003	0.030	2.31	794
MPP2a	45.7	1.214	−0.003	0.027	2.31	664

The XPS O1s core level spectra of copolymer coated nanoparticles, MPP1a and MPP1b, show two different contributions for the lattice oxygen. The first one, the main contribution, centered at 530.0 eV, is due to oxygen in the spinel ferrite structure. The second contribution, centered at 530.9 eV, could be attributed to under-coordinated lattice oxygen, suggesting structural defects (Fig. 4c). The contribution of the first peak to the XPS O1s intensity is around 76% for the copolymer coated nanoparticles. The presence of copolymer around the iron oxide nanoparticle is sustained by the O1s peaks at 531.8 eV and 533.0 eV, assigned to C=O and C–O bonds.

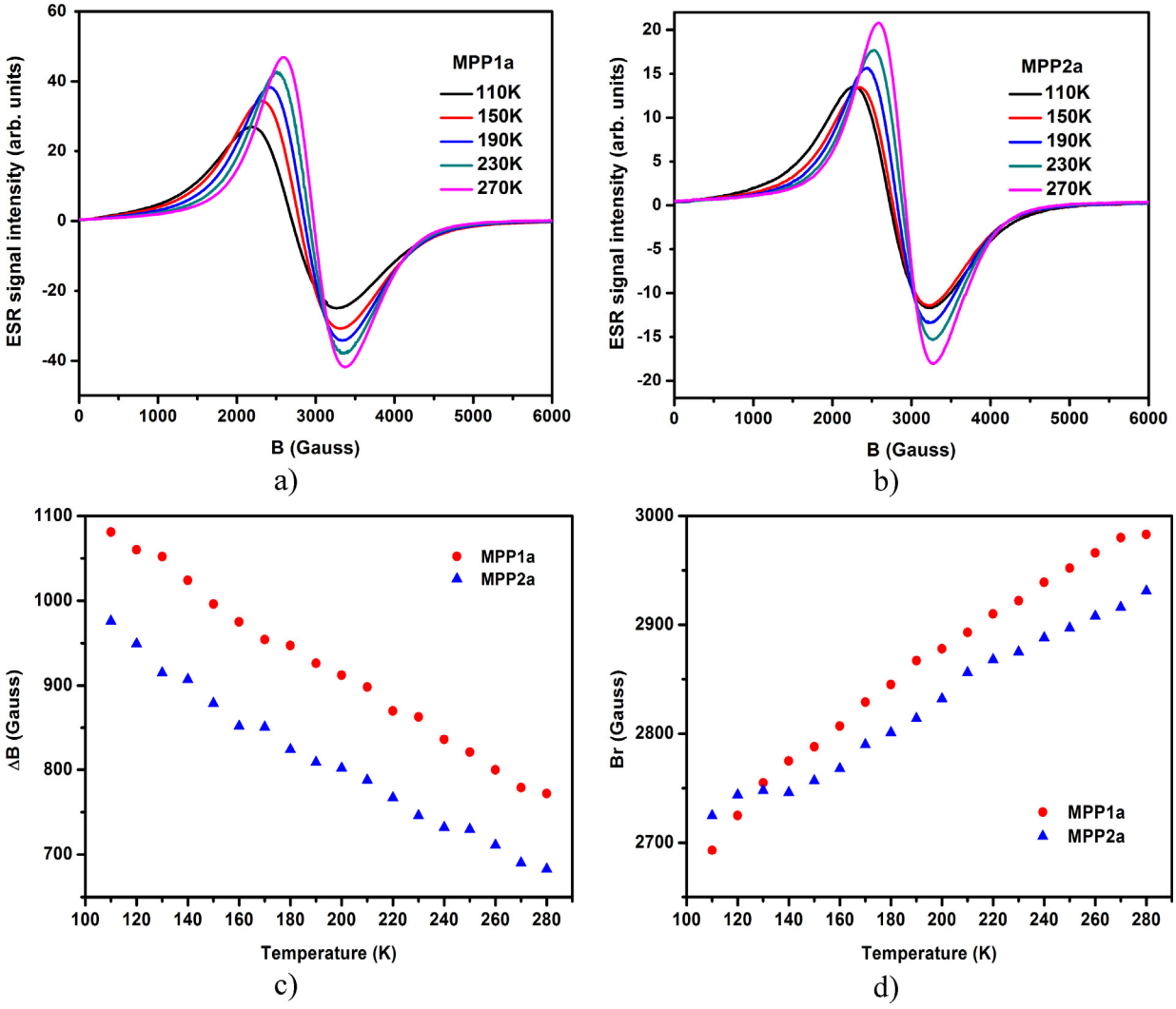

Fig. 6. Temperature dependence of ESR spectra (a and b), ESR signal linewidth (ΔB) (c), and the resonance field (Br) (d).

The XPS spectrum of C1s was decomposed into five XPS peaks, as shown in Fig. 4c. The peaks at 284.4, 284.5, 285.7, 286.7, and 288.5 eV indicate carbon atoms with different chemical environments, typical for AAc-co-MMA.

3.2. Magnetic properties

Magnetic properties were studied at room temperature using a Model 3900 Vibrating Sample Magnetometer System (VSM). Also, the electron paramagnetic resonance (EPR) spectra have been provided by an E500 Elexsys CW-EPR Spectrometer from Bruker, as a function of temperature, in the range 110–340 K.

It is know that when the size of an ultra fine magnetic crystallite is below a critical value, it has only one magnetic domain and shows superparamagnetism. Due to the fact that the size values of prepared nanoparticles are below 25 nm, the superparamagnetic nature is expected. The magnetic hysteresis loops were registered by changing continuously the magnetic field between +10 and −10 kOe. It can be seen that the three cycles do not show hysteresis which demonstrates the superparamagnetic behavior of nanoparticles in all cases (Fig. 5).

The values of magnetic parameters of the samples are presented in Table 4. It is noted that remanent magnetization and saturation magnetization increase significantly with polymer coating, while the coercitive field has negligible values. The coercive field values are similar and this can be attributed mainly to similar morphology of all the nanoparticles and also the lack of shape anisotropy.

EPR spectra of aged nanoparticles, registered at room temperature in X band, show a dependence on iron oxide phases, on particle grain size and on the ratio surfactant/copolymer. The large signal at $g = 2.41$ is typical for maghemite nanostructures. It can be seen that the EPR signal line-width and the amplitude decreases with increasing surfactant concentration in MPP1a sample, but especially with increasing polymer concentration in MPP2a sample. Thus, the dipolar interactions between the MPs are reduced by surfactant and polymer layers, and this could cause a change in line-width and amplitude of EPR signal [49].

Regarding EPR analysis, as one can see in Fig. 6a, b, in each sample, decreasing temperature makes broad component to widen and shift weakly to lower fields. EPR spectra shape and its evolution with temperature are similar to those observed for Fe_3O_4 and γ-Fe_2O_3 particles by other authors [45,46]. Pronounced broadening of the EPR spectra may occur from a wide size and shape distribution and, mainly, an increment of the effective anisotropy and the presence of interactions between particles [47,48,50]. EPR studies have shown that in systems consisting of magnetic nanoparticles dipole–dipole interactions poorly affects the resonance field, while a fast decrease of it is given by exchange coupling of the nanoparticle moments [51].

Not least, it may be mentioned the action of polymer and surfactant layers on MPs, creating between them a magnetoelastic effect caused by stress exerted on particle due to elastic deformation of the polymer, process that can be enhanced at temperatures below 120 K. Therefore, the surface anisotropy of the MPs it may occur, triggering the fast resonance field shift. If we look at graphs in Fig. 6a, b, in any of the samples there is no significant shifts of the EPR shape spectra because of the magnetoelastic effect. Also elastic stress increases strength interactions by reducing the distance between nanoparticles and could even intensify exchange coupling by bringing into close contact nanoparticles in aggregates. It is evident from the EPR spectra that in our samples these processes do not happen because the nanoparticles in all the samples have a good dispersion due to surfactant, thus, preventing the nanoparticles approaching, interplay of polymer layers and formation of agglomerates.

Fig. 6c shows the results of temperature studies of the EPR spectral characteristics of synthesized particles. As one can see, MPP1a and MPP2a samples, demonstrate broadening upon cooling and that the EPR peak-to-peak line-width ΔB increases almost linearly with temperature decreasing. An explanation of this linearity is that the magnetization is temperature dependent due to the increases of magnetic moments of the individual particles.

EPR resonance field values as function of temperature can be observed in Fig. 6d. It is clear that with the temperature decreasing the resonance field decreases monotonically up to 130–140 K for all samples. At this temperature is found a descent of the EPR resonance field very likely due to decreasing of the magnetic anisotropy below 140 K. This aspect has been found also in other studies on magnetic particles [52].

4. Conclusions

The emulsion polymerization method was used to synthesize three sample of polymer coated magnetic particles obtained before through co-precipitation technique. The prepared PMMA-co-AAc coated magnetic particles have spherical shape, nanometric dimensions without agglomerations. The coated and uncoated magnetite nanoparticles were stored for two years in normal closed ships. It has been shown that morphology changes were found only in the case of aged uncoated magnetite nanoparticles.

The FTIR spectra of uncoated magnetic nanoparticles, evidence the vibration bands typical for nonstoichiometric magnetite. In the coated magnetic nanoparticles could be observed a shift of magnetite characteristic peaks to higher wavenumbers as a function of the surfactant/polymer ratio due to the interaction between magnetite and polymer layer induces. Also, the spectral characteristics of PMMA-co-AAc were present. The FTIR spectra of aged nanoparticles shows more visible vibration bands attributed to the copolymer due to the major loss in water content in comparison to the as prepared ones.

The XRD pattern of the aged uncoated nanoparticles shows a mixture of magnetite and maghemite phases. For the aged copolymer coated nanoparticles only the diffraction peaks of spinel structure typical for magnetite is presented.

The presence of magnetite and an important maghemite content was evidenced from Fe2p XPS spectra of aged copolymer coated and uncoated nanoparticles, respectively. The Fe^{2+}/Fe^{3+} ratio in magnetite and the relative contributions of Fe^{3+} ions in octahedral and tetrahedral sites were determined. A diminution in the content of tetrahedral Fe^{3+} lattice sites was evidenced due to the interaction with the copolymer. The concentration in maghemite phase was found to be 69.6%, very close to the value obtained from XRD. The presence of copolymer around the iron oxide nanoparticle is sustained by the O1s peaks assigned to C=O and C–O bonds. The XPS spectrum of C1s indicates the presence of carbon atoms with different chemical environments, typical for AAc-co-MMA.

Magnetic measurements evidenced the superparamagnetic behavior of the nanoparticles. The room temperature EPR spectra revealed that the dipolar interactions between particles are very weak due to the presence of polymer on the nanoparticles surfaces. Thus, embedding has a strong effect on Fe_3O_4 particles decreasing inter-particle interactions. The temperature dependences of the EPR peak-to-peak line-width and the resonance field are typical for magnetic particles. As seen, from the temperature dependence of the resonance field the presence of polymer has not modified essentially its magnetic properties, except that at temperatures below 140 K there was a change due to decreasing of the magnetic anisotropy.

All these analysis demonstrate that PMMA-co-AAc coated magnetic nanoparticles are suitable for biomedical applications.

Acknowledgments

This work was supported by the strategic grant POSDRU/159/1.5/S/137750, "Project Doctoral and Postdoctoral programs support for increased competitiveness in Exact Sciences research" cofinanced by the European Social Found within the Sectorial Operational Program Human Resources Development 2007–2013.

The authors also would like to thank Professor Alfonso Nastro and PC_SM Mario Terenzi Laboratory Research Group at Department of Chemistry and Chemical Technology, University of Calabria, Italy for their scientific advices and support.

References

[1] R. Weissleder, A. Bogdanov, E.A. Neuwelt, M. Papisov, Adv. Drug Deliv. Rev. 16 (1995) 321–334.
[2] L.F. Gamarra, G.E.S. Brito, W.M. Pontuschka, E. Amaro, A.H.C. Parma, G.F. Goya, J. Magn. Magn. Mater. 289 (2005) 439–441.
[3] D.L.J. Thorek, A.K. Chen, J. Czupryna, A. Tsourkas, Ann. Biomed. Eng. 34 (2006) 23–38.
[4] H. Lee, E. Lee, D.K. Kim, N.K. Jang, Y.Y. Jeong, S. Jon, J. Am. Chem. Soc. 128 (2006) 7383–7389.
[5] R. Qiao, C. Yang, M. Gao, J. Mater. Chem. 19 (2009) 6274–6293.
[6] K.A. Radermacher, S. Boutry, S. Laurent, L. Vander Elst, I. Mahieu, C. Bouzin, J. Magat, V. Gregoire, O. Feron, R.N. Muller, B.F. Jordan, B. Gallez, Contrast Media Mol. Imaging 5 (2010) 258–267.
[7] J. Lodhia, G. Mandarano, N.J. Ferris, P. Eu, S.F. Cowell, Biomed. Imaging Interv. J. 6 (2010) e12.
[8] F. Yu, L. Zhang, Y. Huang, K. Sun, A.E. David, V.C. Yang, Biomaterials 31 (2010) 5842–5848.
[9] R. Hergt, S. Dutz, R. Müller, M. Zeisberger, J. Phys.: Condens. Matter 18 (2006) S2919–S2934.
[10] J. Fortin, C. Wilhelm, J. Servais, C. Ménager, J. Bacri, F. Gazeau, J. Am. Chem. Soc. 129 (2007) 2628–2635.
[11] G. Nedelcu, Dig. J. Nanomater. Bios. 3 (2008) 99–102.
[12] G. Nedelcu, Dig. J. Nanomater. Bios. 3 (2008) 103–107.
[13] R. Sharma, A. Sharma, C.J. Chen, Open Nanomed. J. 3 (2011) 10–23.
[14] S. Laurent, S. Dutz, U.O. Häfeli, M. Mahmoudi, Adv. Colloid Interface Sci. 166 (2011) 8–23.
[15] Q. Zhao, L. Wang, R. Cheng, L. Mao, R.D. Arnold, E.W. Howerth, Z.G. Chen, S. Platt, Theranostics 2 (2012) 113–121.
[16] V.P. Torchilin, Eur. J. Pharm. Sci. 11 (2000) S81.
[17] A.K. Gupta, S. Wells, IEEE Trans. Nanobiosci. 3 (2004) 66–73.
[18] P.V. Finotelli, D. Da Silva, M. Sola-Penna, A. Malta Rossi, M. Farina, L. Rodrigues Andrade, A. Yoshihaki Takeuchi, M.H. Rocha-Leão, Colloids Surf. B: Biointerfaces 81 (2010) 206–211.
[19] S. Xuan, F. Wang, J.M.Y. Lai, K.W.Y. Sham, Y-X.J. Wang, S.-F. Lee, J.C. Yu, C.H.K. Cheng, K.C.-F. Leung, ACS Appl. Mater. Interface 3 (2011) 237–244.
[20] A.K. Gupta, M. Gupta, Biomaterials 26 (2005) 3995–4021.
[21] M. Babic, D. Horák, M. Trchová, P. Jendelová, K. Glogarová, P. Lesnyí, V. Herynek, M. Hájek, E. Syková, Bioconjug. Chem. 19 (2008) 740–750.
[22] G.P. Vonk, J.L. Schram, J. Immunol. Methods 137 (1991) 133–139.
[23] J.M. Nam, C.S. Thaxton, C.A. Mirkin, Science 301 (2003) 1884–1886.
[24] A. Bhirde, J. Xie, M. Swierczewska, X. Chen, Nanoscale 3 (2011) 142–153.
[25] I. Koh, L. Josephson, Sensors 9 (2009) 8130–8145.
[26] E. Druet, P. Mahieu, J.M. Foidart, P.J. Druet, Immunol. Methods 48 (1982) 149–157.
[27] S. Lu, R. Qu, J. Forcada, Mater. Lett. 63 (2009) 770–772.
[28] S. Wu, A. Sun, F. Zhai, J. Wang, W. Xu, Q. Zhang, A.A. Volinsky, Mater. Lett. 65 (2011) 1882–1884.
[29] Y. Liu, Z.F. Gao, Q. Sun, Y.P. Zeng, Hyperfine Interact. 219 (2013) 107–112.
[30] M.C. Mascolo, Y. Pei, T.A. Ring, Materials 6 (2013) 5549–5567.
[31] S. Chkoundali, S. Ammar, N. Jouini, F. Fievet, P. Molinie, M. Danot, F. Villain, J.-M. Greneche, J. Phys.: Condens. Matter 16 (2004) 4357–4372.
[32] A.C. Druc, A.I. Borhan, G.G. Nedelcu, L. Leontie, A.R. Iordan, M.N. Palamaru, Mater. Res. Bull. 48 (2013) 4647–4654.
[33] A.C. Druc, A.I. Borhan, A. Diaconu, A.R. Iordan, G.G. Nedelcu, L. Leontie, M.N. Palamaru, Ceram. Int. 40 (2014) 13573–13578.
[34] H. Srikanth, R. Hajndl, C. Chirinos, J. Sanders, A. Sampath, T.S. Sudarshan, Appl. Phys. Lett. 79 (2001) 3503–3505.
[35] Y. Zhang, N. Kohler, M. Zhang, Biomaterials 23 (2002) 1553–1561.
[36] Z. Guo, L.L. Henry, V. Palshin, E.J. Podlaha, J. Mater. Chem. 16 (2006) 1772–1777.
[37] F. Sayar, G. Güven, E. Pişkin, Colloid Polym. Sci. 284 (2006) 965–978.
[38] L. Zhou, J. Yuan, W. Yuan, X. Sui, S. Wu, Z. Li, D. Shen, J. Magn. Magn. Mater. 321 (2009) 2799–2804.
[39] L.G. Bach, M.R. Islam, J.T. Kim, S. Seo, K.T. Lim, Appl. Surf. Sci. 258 (2012) 2959–2966.
[40] Z. Tang, X. Wang, L. Pan, Y. Hu, Y. Wu, J. Zhang, S. Cui, J. Kang, J. Tang, Adv. Mater. Res. 647 (2013) 155–159.
[41] Y. Zhu, Q. Wu, J. Nanopart. Res. 1 (1999) 393–396.
[42] Y. Sun, M. Ma, Y. Zhang, N. Gu, Colloids Surf. A 245 (2004) 15–19.
[43] E. Tombácz, E. Illés, A. Majzik, A. Hajdú, N. Rideg, M. Szekeres, Croat. Chem. Acta 80 (3–4) (2007) 503–515.
[44] L.P. Ramirez, K. Landfester, Macromol. Chem. Phys. 204 (2003) 22–31.
[45] H. Bagheri, O. Zandi, A. Aghakhani, Anal. Chim. Acta 692 (2011) 80–84.
[46] S. Nasrazadani, A. Raman, Corros. Sci. 34 (8) (1993) 1355–1365.
[47] M.M. Noginov, N. Noginova, O. Amponsah, R. Bah, R. Rakhimov, V.A. Atsarkin, J. Magn. Magn. Mater. 320 (2008) 2228–2232.
[48] N. Noginova, F. Chen, T. Weaver, E.P. Giannelis, A.B. Bourlinos, V.A. Atsarkin, J. Phys.: Condens. Matter 19 (2007) 246208.
[49] H. Kavas, N. Kasapoğlu, A. Baykal, Y. Köseoğlu, Chem. Papers 63 (2009) 450–455.
[50] Y.A. Koksharov, S.P. Gubin, I.D. Kosobudsky, G.Yu. Yurkov, D.A. Pankratov, L.A. Ponomarenko, M.G. Mikheev, M. Beltran, Y. Khodorkovsky, A.M. Tishin, Phys. Rev. B 63 (2000) 012407.
[51] R. Berger, J.C. Bissey, J. Klava, H. Daubric, C. Estournes, J. Magn. Magn. Mater. 234 (2001) 535–544.
[52] V.N. Nikiforov, Y.A. Koksharov, S.N. Polyakov, A.P. Malakho, A.V. Volkov, M.A. Moskvina, G.B. Khomutov, V.Y. Irkhin, J. Alloys Compd. 569 (2013) 58–61.